

# Controlled Jamming of Particle-Laden Interfaces Using a Spinning Drop Tensiometer

Hsin-Ling Cheng and Sachin S. Velankar\*

*Department of Chemical Engineering, University of Pittsburgh, Pittsburgh, Pennsylvania 15261**Received October 24, 2008. Revised Manuscript Received January 8, 2009*

When particles adsorb at a fluid/fluid interface at a sufficiently high concentration, the interface loses mobility and displays solidlike characteristics, a phenomenon called “interfacial jamming”. Jamming can arrest interfacial tension-driven morphological coarsening in liquid/liquid or gas/liquid systems and therefore stabilize two phase morphologies with unusual interfacial shapes, for example, nonspherical drops and bijels. Here, we conduct a systematic study of interfacial tension-driven jamming of a particle monolayer using a spinning drop tensiometer (SDT). A drop of mineral oil surrounded by ethylene glycol was spun into a cylindrical shape in a SDT. With decreasing rotational rate, the cylindrical drop retracted due to interfacial tension, thus reducing the interfacial area. In the case of particle-covered drops, drop retraction caused an increase in interfacial particle concentration. Accordingly, when the specific interfacial area became comparable to that of a close packing of particles, interfacial jamming occurred and drop retraction was arrested. Fast interfacial contraction or low particle loadings led to less compact jammed monolayers, that is, with a larger specific interfacial area. There was also significant hysteresis between compressing versus expanding the jammed monolayer, suggesting that a certain minimum stress is required for unjamming.

Limited experiments with the same particles at a mineral oil/silicone oil interface showed altogether different behavior. In this case, particles did not spread at the interface and a particle-free portion of the interface coexisted with a particle-covered portion. This suggests that the monolayer behavior at this nonpolar/nonpolar interface is dominated by interparticle attraction.

## 1. Introduction

Particles that are partially wetted by two immiscible fluids tend to adsorb at the interface between the fluids to minimize the overall free energy of the system. Such interfacially adsorbed particles behave similar to surfactants in some respects, and like some surfactants they can stabilize two-phase emulsions and foams.<sup>1,2</sup> Such emulsions are called Pickering emulsions.<sup>3</sup>

In many cases, the desorption energy for a particle adsorbed at the interface far exceeds the thermal energy,  $kT$ , and hence, particle adsorption is practically irreversible. As particle concentration at the interface is increased, the particles become increasingly crowded at the interface, and eventually lose mobility, a state that has been dubbed as a “jammed” particle monolayer.<sup>4</sup> A jammed monolayer can be solidlike with significant mechanical robustness, and one of its remarkable consequences is the existence of stable nonspherical drops or bubbles:<sup>5</sup> in effect, the nonuniform capillary stresses associated with a nonspherical bubble shape are supported by localized stresses in the solidlike monolayer.

An especially interesting example of stable nonspherical structures in fluid/fluid systems are bicontinuous interfacially jammed emulsion gels (dubbed “bijels”<sup>4</sup>). Bijels are composite materials composed of two immiscible fluids arranged in a

bicontinuous morphology, with a jammed monolayer of particles adsorbed at the interface between them. Bijels can be prepared by starting with a bicontinuous morphology with interfacially adsorbed particles, and then letting interfacial tension cause domain coarsening and hence a decrease in interfacial area. If particles do not desorb during the coarsening process, the interfacial concentration of the particles is expected to rise until jamming occurs, thus stabilizing the bicontinuous morphology. A particularly attractive feature of bijels is the possibility of tuning the size-scale of the morphology via the particle loading. Indeed, in the simplest picture, one may postulate that jamming is associated with a specific interfacial concentration. In that case, the interfacial area per unit volume (which may be regarded as the reciprocal of the domain size of the bijel) would be proportional to the particle loading. Bijels have received increasing attention<sup>4,6–8</sup> because of their unusual bicontinuous morphology, since, except some microemulsions, the bicontinuous morphology is usually not stable in liquid systems.

In this paper, we undertake a fundamental study of interfacial tension-driven interfacial jamming at the liquid/liquid interface, which has relevance to bijel formation. The key to study jamming systematically is to decrease the interfacial area in a controlled fashion. Past experiments have principally used two methods to reduce the interfacial area systematically. The first is a Langmuir trough (Figure 1a), in which a physical barrier (or two barriers for symmetric compression) is moved

(1) Binks, B. P. *Curr. Opin. Colloid Interface Sci.* **2002**, 7(1–2), 21–41.

(2) Binks, B. P.; Horozov, T. S. *Colloidal particles at liquid interfaces*; Cambridge University Press: Cambridge, **2006**.

(3) Pickering, S. U. *J. Chem. Soc., Trans.* **1907**, 91, 2001–2021.

(4) Stratford, K.; Adhikari, R.; Pagonabarraga, I.; Desplat, J. C.; Cates, M. E. *Science* **2005**, 309(5744), 2198–2201.

(5) Subramaniam, A. B.; Abkarian, M.; Mahadevan, L.; Stone, H. A. *Nature* **2005**, 438(7070), 930–930.

(6) Chung, H.; Ohno, K.; Fukuda, T.; Composto, R. J. *Nano Lett.* **2005**, 5(10), 1878–1882.

(7) Si, M.; Araki, T.; Ade, H.; Kilcoyne, A. L. D.; Fisher, R.; Sokolov, J. C.; Rafailovich, M. H. *Macromolecules* **2006**, 39(14), 4793–4801.

(8) Herzig, E. M.; White, K. A.; Schofield, A. B.; Poon, W. C. K.; Clegg, P. S. *Nat. Mater.* **2007**, 6(12), 966–971.

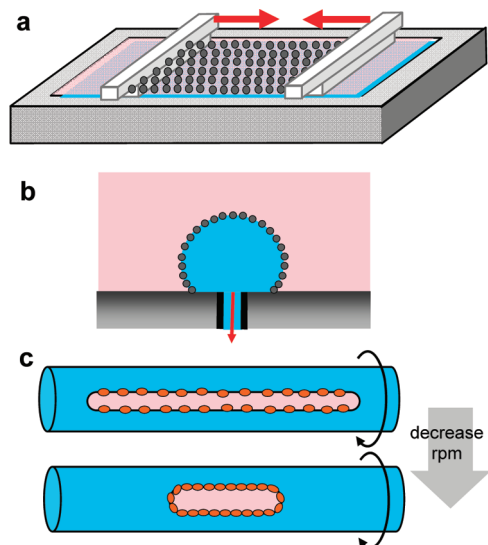


**Figure 1.** Summary of experimental methods to study properties of particle monolayers and interfacial jamming. (a) Langmuir trough, (b) sessile drop, and (c) spinning drop tensiometer.

to compress the particle monolayer.<sup>9–12</sup> In this case, the compression is driven from the edges of the monolayer and the nominal interfacial area is directly controlled. In such experiments, jamming can occur if the monolayer is compressed sufficiently. Further decrease in the nominal interfacial area can cause interfacial buckling (an out-of-plane distortion or wrinkling of the monolayer); that is, the nominal interfacial area becomes smaller than the actual area. The second method is a shrinking drop (or bubble) method, in which the monolayer is placed on the surface of a pendant or sessile drop and fluid is withdrawn from the drop (Figure 1b).<sup>13–15</sup> In this case, the volume of the drop (rather than the area) is directly controlled. The drop shape follows the Laplace–Young equation, and hence, the interfacial area reduces in a predictable fashion, at least as long as the interface remains unjammed. In these experiments as well, sufficient withdrawal of the drop phase fluid can induce interfacial jamming, and further withdrawal can be accompanied by interfacial buckling.<sup>13–15</sup>

There are however several differences between interfacial jamming during bijel formation and interfacial jamming in a Langmuir trough or on a shrinking drop. Unlike in the two methods of Figure 1a and b, the bicontinuous interface in a bijel does not have physical barriers, nor does the volume of the fluid change. The driving force for the decrease in interfacial area in a bijel is interfacial tension or, more precisely, gradients in capillary pressure due to difference in curvature along the interface. This mechanism is different from a shrinking drop or especially different from compression in a

Langmuir trough. Furthermore, during bijel formation, the interfacial driving force remains nearly constant (or decreases) during the coarsening process, whereas properties such as interfacial viscosity or modulus increase as the particles pack more closely. Therefore, the rate of decrease in interfacial area is expected to reduce as jamming is approached. In contrast, in a Langmuir trough or a shrinking drop, the area is decreased at a prescribed rate. Finally, we hypothesize that buckled states, which result from trying to decrease the area below that required for jamming, are unlikely to occur in bijels, since interfacial coarsening is expected to stop once the interfacial yield stress approaches the interfacial tension driving force.

Here, we propose an alternate method of reducing the interfacial area that is more representative of the jamming process in bijels. Specifically, as in bijels, in the proposed method, the decrease in interfacial area is induced by interfacial tension. The method uses the spinning drop tensiometer (SDT, Figures 1c and 2). When two fluids are spun in a tube along a horizontal axis, the lower density fluid “centrifuges” to the center and stretches into a cylindrical drop. The drop shape at equilibrium results from a balance between interfacial stress ( $\sim\sigma/R$ ) and centrifugal stress ( $\sim\Delta\rho R^2\Omega^2$ ). It has been shown that at equilibrium<sup>16</sup>

$$\sigma = \frac{\Delta\rho R^3\Omega^2}{4} \quad \text{provided} \quad \left(\frac{L}{2R} > 4\right) \quad (1)$$

where  $\Delta\rho$  is the density difference of the two fluids,  $2R$  is the diameter of the cylindrical drop,  $L$  is its length,  $\sigma$  is the interfacial tension, and  $\Omega$  is the rotational rate. The above equation is called Vonnegut’s formula and is the basis for using the SDT to measure the interfacial tension between immiscible fluids. The SDT has also been used less frequently to examine the dynamics of interfacial-tension-driven drop shape changes in fluids. Specifically, by first preparing a long drop at high rotational speed and then abruptly reducing the rotational speed, the retraction<sup>17,18</sup> or capillary breakup<sup>19</sup> of a drop can be studied.

Such changes in drop shape with rotational speed can also be used to change the interfacial area systematically. Specifically, as the rotational speed is reduced, the drop retracts and the interfacial area of the drop reduces in a predictable fashion. By covering the surface of the drop with a particle monolayer, the decrease in interfacial area may be used to induce interfacial jamming. Most importantly, as in bijels, the decrease in interfacial area and the eventual jamming is driven by interfacial tension/capillary pressure. Other similarities with bijel jamming include the absence of physical barriers, the absence of spreading solvent, and the geometric analogy between an elongated drop and the fluid channels (the necks) in a bijel. In summary, the SDT method of Figure 1c is more representative of the eventual jamming of a bijel than the methods of Figure 1a and b.

In this paper, we study interfacial particle jamming experimentally in a well-controlled manner using a spinning drop tensiometer. Our previous research<sup>20</sup> on particle monolayers

(9) Aveyard, R.; Clint, J. H.; Nees, D.; Quirke, N. *Langmuir* **2000**, *16*(23), 8820–8828.

(10) Aveyard, R.; Clint, J. H.; Nees, D.; Paunov, V. N. *Langmuir* **2000**, *16*(4), 1969–1979.

(11) Horozov, T. S.; Aveyard, R.; Clint, J. H.; Binks, B. P. *Langmuir* **2003**, *19*(7), 2822–2829.

(12) Basavaraj, M. G.; Fuller, G. G.; Fransae, J.; Vermant, J. *Langmuir* **2006**, *22*(15), 6605–6612.

(13) Xu, H.; Melle, S.; Golemanov, K.; Fuller, G. *Langmuir* **2005**, *21*(22), 10016–10020.

(14) Monteux, C.; Kirkwood, J.; Xu, H.; Jung, E.; Fuller, G. G. *Phys. Chem. Chem. Phys.* **2007**, *9*(48), 6344–6350.

(15) Asekomhe, S. O.; Chiang, R.; Masliyah, J. H.; Elliott, J. A. W. *Ind. Eng. Chem. Res.* **2005**, *44*(5), 1241–1249.

(16) Vonnegut, B. *Rev. Sci. Instrum.* **1942**, *13*, 6–9.

(17) Martin, J. D.; Velankar, S. Effect of surfactant on the viscous Raleigh-Tomotika instability. In preparation.

(18) Martin, J. D.; Velankar, S. S. *J. Colloid Interface Sci.* **2008**, *322*(2), 669–674.

(19) de Hoog, E. H. A.; Lekkerkerker, H. N. W. *J. Phys. Chem. B* **2001**, *105*(47), 11636–11640.

(20) Cheng, H. L.; Velankar, S. S. *Colloids Surf., A* **2008**, *315*(1–3), 275–284.

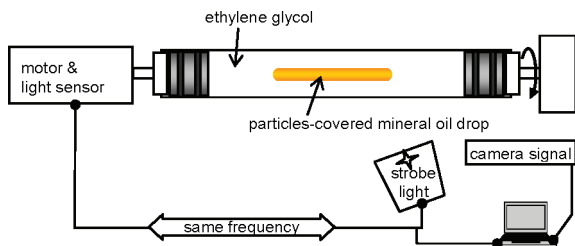


**Figure 2.** SDT experimental setup. The strobe light and the rotor are operated under the same frequency by synchronizing the signal through a light sensor. A camera (not shown) takes live images from above.

suggests that the adsorption of iron oxyhydroxide particles (FeOOH) onto the interface of mineral oil and ethylene glycol is fast, stable, and convenient for visual observation because of the intense yellow color of the particles.<sup>20</sup> In this paper, a FeOOH-particle-covered drop of mineral oil suspended in ethylene glycol was spun in the SDT, and jamming was induced by decreasing the rotational rate and hence the interfacial area. Since the particle loading is known for a given sample, we can relate the interfacial particle concentration with rotational rate and deduce the conditions under which jamming occurs for different samples. We study the gradual jamming (slow decrease in area) and also the “dynamic” jamming (rapid decrease in area), and the effect of rotational rate history. We also show that the same particle monolayer at a nonpolar/nonpolar interface behaves completely differently from that at the glycol/oil interface. This study about the physics of jamming is intended to serve as the foundation for structure control through interfacial particle jamming in bijels.

## 2. Materials and Experiments

**2.1. Materials.** Light mineral oil was obtained from Fisher Scientific Inc. Its density was determined to be 0.854 g/mL by weighing in a pycnometer vial. Ethylene glycol was also obtained from Fisher. Silicone oil (polydimethylsiloxane, Rhodorsil fluid 47 V10,000), obtained from Rhodia Inc., has a viscosity and density of 10 Pa·s and ca. 0.96 g/mL, respectively.

Iron oxyhydroxide (FeOOH) particles were donated by Elementis Pigments Inc. The particles are polydisperse, elongated with an average length of about 0.6  $\mu\text{m}$  (manufacturer specified), have a density of 4.03 g/cm<sup>3</sup> (manufacturer specified), and appear yellow in color. A scanning electron microscopy (SEM) picture of the particles is shown in Figure 6c. These same particles were used in our previous research.<sup>20</sup>

**2.2. Sample Preparation and Experimental Procedure.** FeOOH particles of a carefully weighed amount were first dispersed in mineral oil using ultrasonication for 10 min and followed by short vortex mixing. Three suspensions with the concentrations listed in Table 1 were prepared. In each case, the suspension was transferred to a syringe, and roughly 0.073 mL was injected into the precision-bore sample tube filled with degassed ethylene glycol. The exact volumes of the drops (calculated numerically from drop images; see below) and the corresponding particle loadings are also listed in Table 1.

The tube (12.7 mm diameter, 165 mm long) was closed with an endplug, mounted in the SDT, and spun in the tensiometer at a high rotational rate. Since the particles are denser than the oil, they migrate to the interface and get adsorbed. To prevent a multilayer of particles from forming at the interface, the tube was taken out from the tensiometer, held horizontally, and shaken gently so that particles not adsorbed at the interface would be dispersed back to the drop phase. The tube was then spun in the SDT again. This rotation and shaking was repeated

several times until the bulk drop phase appeared clear and there was no further change in drop dimensions at a fixed rpm. Throughout this procedure, the matrix phase (ethylene glycol) as well as the inner surface of the glass tube appeared to be clear, suggesting that no particle penetrates through the interface without being adsorbed.

After particles had been adsorbed at the interface, each sample was first brought to high rotational rate (e.g., 7000 rpm), and then the rotational speed was decreased in roughly 250 rpm decrements. After each change in rotational rate, images were taken after no less than 2 min to ensure that the drop shapes had reached steady state. To confirm that the drop shape images taken at the 2 min waiting time are indeed the steady drop shapes, we monitored one sample for 24 h and confirmed that the drop dimensions did not change after the first 2 min. This procedure of sequentially decreasing the rotational speed is dubbed the “ratedown” experiment.

Some samples were also subjected to a subsequent “rateup” experiment in which the rotational speed was increased in roughly 250 rpm increments.

An “abrupt stepdown” experiment was also conducted on the F71 sample, in which the rotational rate was decreased abruptly from roughly 6500 to 1500 rpm within a few seconds. Dynamics of the drop retraction during this experiment was recorded as a sequence of still images.

Similar experiments were conducted with FeOOH particles adsorbed at the mineral oil/silicone oil interface. In this case as well, the mineral oil has a lower density and hence forms the drop phase; thus, once again, the particles were dispersed into the mineral oil and then allowed to centrifuge to the interface. Because mineral oil has slight solubility in silicone oil, the matrix phase silicone oil was presaturated with mineral oil as follows: mineral oil drops were gently blended into silicone oil and then allowed to float to the surface over several hours. The bottom layer silicone oil, now saturated with mineral oil, was used as the matrix phase. The interfacial tension between the equilibrated phases was measured by the pendant drop experiment. The value calculated using the densities of the pure oils was 1.05 mN/m; the equilibrated phases likely have a somewhat lower density difference, and hence, the above number is likely an overestimate. In any case, this interfacial tension is far lower than the value of  $\sim 17.6$  mN/m measured for the glycol/oil system (see below) and reflects the low polarity of both species.

**2.3. Imaging and Image Analysis.** The experimental setup is shown in Figure 2 schematically. Images were taken with a video zoom lens and a digital camera (EO-1312M), with the exposure time set to 0.1 s. The tube was illuminated by a strobe light, which was triggered by a reflective sensor detecting the rotating shaft of the SDT. The signal from the reflective sensor was also used to record the rotational rate using a Labview interface. The cylindrical tube of the SDT causes optical lensing, making spherical objects appear stretched along the tube diameter. This “diameter magnification” was calibrated using an image of a spherical polyethylene bead of known dimensions suspended in ethylene glycol in the SDT tube. All the images presented in this paper have been corrected to account for diameter magnification. The optical system has a resolution of slightly less than 50  $\mu\text{m}$ .

Surface area and volume of the drop were calculated by numerical integration of the drop shape profile. The edge of the drop was drawn manually, since automatic edge detection was found to be unreliable, especially when a striped background was used to enhance image quality. The coordinates of the edge were exported and used to calculate surface area and volume with the assumption of axisymmetric drop shape. The numerical calculations were validated by two methods: (1) the interfacial area and volume of the spherical polyethylene bead was compared against numerical calculations, and (2) for all drops, the calculated volume was verified to be independent of rpm.

**Table 1. Drop Volumes and Particle Loadings for Each Sample**

designation	FeOOH wt % in suspension	drop volume (mL)	particle loading ( $\mu\text{g}$ )
particle free	0	0.0755	0
F51	0.08	0.0735	51.5
F62	0.1	0.0728	62.2
F71	0.12	0.0714	71.4

### 3. Results and Discussion

**3.1. Drop Shapes and Apparent Interfacial Tension.** At the initially high rotational rate of the raterdown protocol, drop shapes of all samples are approximately spherocylindrical (cylinder with hemispherical end-caps), and their shapes result from a balance between interfacial and centrifugal forces as implicit in Vonnegut's formula (eq 1).

For the particle-free sample, as rotational rate is reduced, the drop retracts and its radius increases as illustrated in Figure 3a. The corresponding interfacial tension, calculated using Vonnegut's formula, eq 1, is shown in Figure 3b, although many of the datapoints for this sample are obscured by other data that superimpose upon these points. At sufficiently low rpm, the drop radius approaches that of a sphere of the same volume as the original spherocylindrical drop. At very low rotational rate, the shape may also be affected by buoyancy effects. As long as the drop is long ( $L/2R > 4$ ), Vonnegut's formula suggests  $R \propto \Omega^{-2/3}$ . The observed exponent of  $-0.64$  is close to, but not exactly identical, to the  $-0.667$  expected, and accordingly, the interfacial tension appears to decrease slightly with decreasing rpm. It is not clear why this is so. It may be an artifact of the imaging procedure: any blurring of the image causes a larger error at small drop diameter (i.e., at high rpm). (There are two principal reasons for blurring: (1) uncertainty inherent in the finite spatial resolution of the digital camera, and (2) at high rpm, several strobe flashes occur during a single camera exposure of 0.1 s, and hence, any image is a superposition of several images.) In any case, the average interfacial tension between mineral oil and ethylene glycol by the SDT method is 17.5 mN/m, which agrees well with the value 17.6 mN/m obtained from the pendant drop method (Krüss DSA100).

Figure 3a also shows the dependence of  $R$  on rpm for the particle-loaded drops. At high rpm, the radius of the three particle-laden drops is nearly equal to that of the particle-free drop. Upon reducing rotational speed, at some value of rpm, the radii of the particle-laden drops start deviating downward from that of the particle-free drop. The rpm at which the deviation occurs increases with increasing particle loading. As rpm is reduced further, the radii of the particle-laden drops become increasingly insensitive to the rpm, that is, the drop shapes no longer respond significantly to a decreasing rotational speed. This is due to interfacial jamming: the increasingly crowded particle monolayer hinders the drop from reducing its area, thus causing its shape (discussed below), and hence radius, to become insensitive to rotational rate. The drop shape is no longer determined by an equilibrium balance between centrifugal and interfacial forces, but instead depends on the mechanical history that led to the jammed interface. This will be explored further in section 3.3.

We may apply Vonnegut's equation to find the interfacial tension of the particle-laden drops. At high rotational speed, the interfacial tension of the particle-laden interface is very close to that of the bare interface (Figure 3b), thus indicating

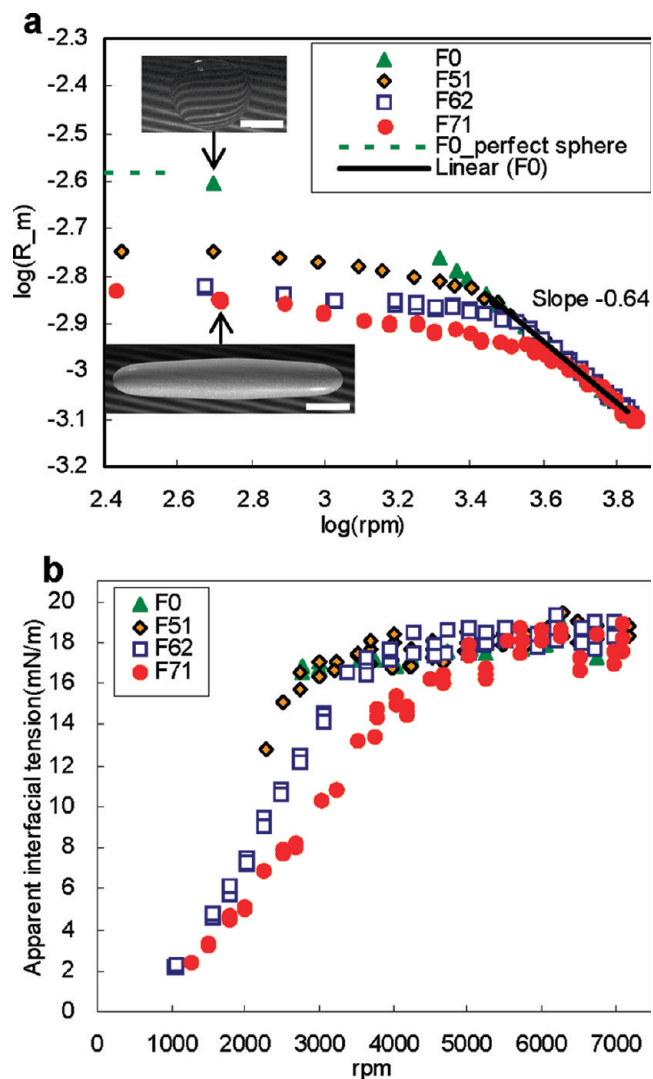


**Figure 3.** (a) Log–log plot of drop radius in meters with rotational rate (rpm). Dashed line shows the radius for a spherical drop of the same volume as the particle-free drop. The scale bar in the insets is 3 mm. (b) Plot of variation of apparent interfacial tension with rpm, calculated from eq 1. Calculation was performed only for drops with aspect ratio  $> 4$ .

that particles do not affect the interfacial tension significantly. At low rotational rates when interfacial jamming occurs, Vonnegut's equation, which assumes a balance between centrifugal forces and interfacial tension, is not strictly valid. Nevertheless, as long as the drop has a cylindrical midsection with an aspect ratio exceeding 4, we may apply Vonnegut's equation to calculate an apparent interfacial tension, which is shown in Figure 3b. The apparent interfacial tension reduces to very low values at low rpm. We emphasize however that this low apparent interfacial tension calculated from eq 1 is not thermodynamically meaningful (hence the “apparent”): the reason for the small radius of the

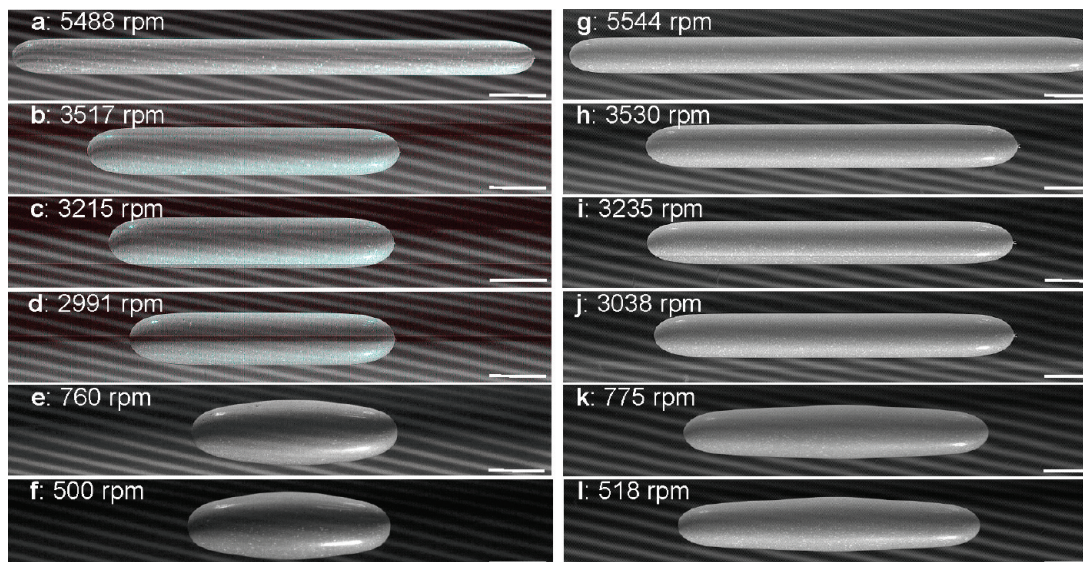


**Figure 4.** Images of F51 (a–f) and F71 (g–l). Scale bars are 3 mm.

drop is not that the interfacial tension is low but that the interface is jammed.

We will now consider the drop shapes in greater detail. Figure 4 shows the evolution of drop shapes with decreasing rpm for the drops with the lowest (F51) and the highest (F71) particle loading. The rotational speeds in Figure 4 were chosen to highlight the differences between the two samples. As mentioned above, all the drop shape images have been corrected to account for the refractive index magnification. At a relatively high rpm of about 5500 (Figure 4a and g), the drop shapes are nearly identical. Upon reducing the rotational rate stepwise to roughly 3500 rpm (b and h), both drops retract significantly. The intermediate shapes are not shown. Upon further decrease in rpm, a qualitative difference is evident: the F51 drop continues to retract (b–d), whereas the F71 drop shows no obvious change in length (h–j) as the rpm is reduced from 3500 to  $\sim 3000$  rpm. The F51 drop continues retracting, and a much lower rotational speed (less than 1000 rpm) is required for its shape to become insensitive to rpm. In this paper, such unchanging drop shape (and hence area) as the rpm reduces is regarded as the signature feature of interfacial jamming. The previous statement needs further qualification. Whether a system jams depends on the stress applied.<sup>21</sup> In the present case, drop retraction is driven by the difference between capillary pressure  $\sim \sigma/R$  (which tends to decrease the interfacial area) and centrifugal stress  $\sim \Delta\rho\omega^2 R^2/4$  (which tends to increase the interfacial area). Thus, the quantity  $(\sigma/R - \Delta\rho\omega^2 R^2/4)$  may be regarded as the interfacial stress driving the drop retraction. As the drop retracts and the interfacial concentration increases, the yield stress of the particle monolayer exceeds the difference between the capillary and the centrifugal stress, and hence, the drop jams.

Upon further and more significant decrease in rotational rate (Figure 4k), the F71 drop does retract further, however, at such low rates, buoyancy effects may contribute to the shape changes. In this case (as well as in the F51 case), at the lowest rotational rates, the drop profile shows a distinct “bump” in its midsection. Can this unusual drop shape be an equilibrium shape (with the force balance

including buoyancy, as well as interfacial, and centrifugal forces)? In section 3.3, we will show there is significant hysteresis in drop shape in this range of rotational rates, and hence such unusual bulging shapes cannot be regarded as equilibrium shapes. Instead, we believe that such unusual shapes are realized by plastic deformation of the jammed monolayer which is induced by buoyancy forces.

In the Introduction we hypothesized that, in interfacial-tension-driven jamming, the interfacial area will stop decreasing once the interfacial yield stress approaches the interfacial tension; accordingly, we hypothesized that interfacial buckling will not occur. Indeed, interfacial buckling is not evident in any of the images of Figure 4. Calculations<sup>22</sup> suggest that, under our jamming conditions with centrifugal accelerations of about  $1\text{--}16\text{ m/s}^2$  (corresponding to the surface our jammed drops), wavelengths of  $100\text{--}400\ \mu\text{m}$  are expected. These dimensions can be readily resolved by our apparatus, and indeed during fast changes in rpm when viscous stresses are significant, we have noted  $100\ \mu\text{m}$  scale ripples on the surface of drops. Yet, under equilibrium conditions, no ripples were evident. This lends tentative support to our hypothesis that monolayers jammed by interfacial tension do not buckle, although buckling at small amplitudes or at wavelengths smaller than  $100\ \mu\text{m}$  cannot be ruled out.

Finally, we note that the jammed drops are stable not only against retraction but also against capillary instabilities. In elongated particle-free drops under quiescent conditions, long-wavelength capillary instabilities that can reduce the interfacial area can grow and eventually lead to drop breakup. However, since jamming prevents a decrease in interfacial area, capillary instabilities are suppressed as well.

**3.2. Interfacial Area, Surface Pressure Isotherm, and Jamming Concentration.** As mentioned in the Introduction, jamming is induced by a decrease in the interfacial area and the consequent increase in particle concentration. The data of Figure 3 have been replotted in Figure 5a in the form of interfacial area of the drop for all four drops. As with the drop radius, all four drops show similar area at high rpm.

(21) Liu, A. J.; Nagel, S. R. *Nature* **1998**, *396*(6706), 21–22.

(22) Vella, D.; Aussillous, P.; Mahadevan, L. *Europhys. Lett.* **2004**, *68*(2), 212–218.

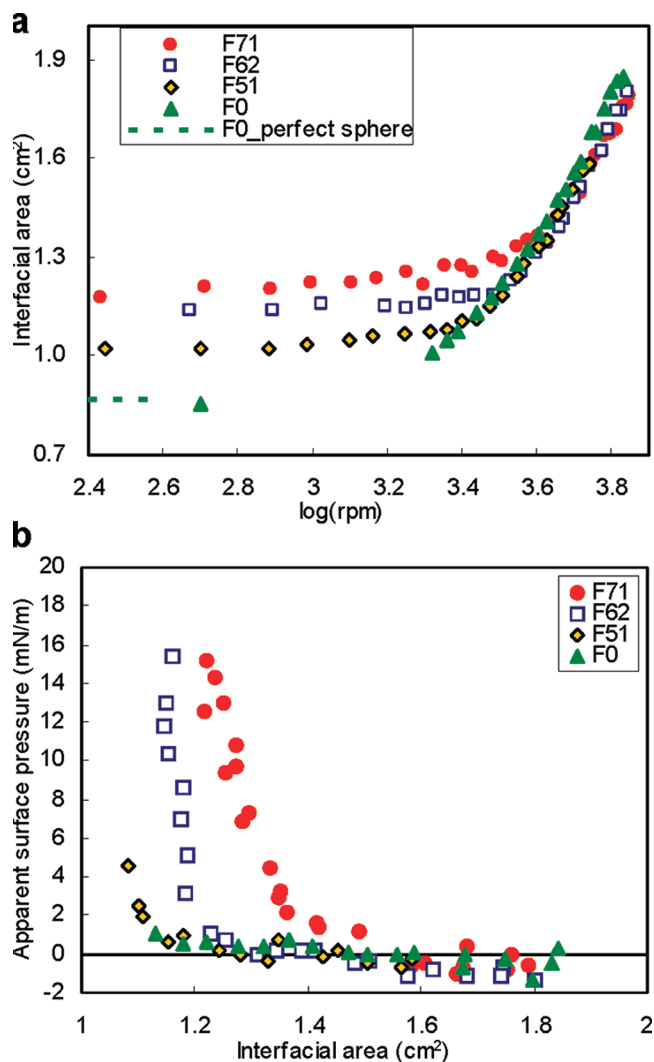


**Figure 5.** (a) Variation of interfacial area with  $\log(\text{rpm})$  for a ratedown experiment. (b) Plot of apparent surface pressure versus interfacial area. See text for explanation for negative apparent surface pressures.

This is not surprising: the four drops have a similar volume, and hence, an equal radius implies equal area as well. At low rpm, the area of the particle-free drop approaches that of a sphere of the same volume. The area versus rpm data for all three particle-laden drops deviates upward from the particle-free drops at low rpm, with two trends evident: First, the rpm (and hence the area) at which the deviation occurs increases with particle loading. Second, the plateau value of the area at low rpm increases with particle loading.

In experiments conducted in a Langmuir trough, it is traditional to represent the data in the form of surface pressure versus area isotherms, and it is of interest to represent our data in the same form. The apparent interfacial tension,  $\sigma_{\text{apparent}}$ , can be calculated from eq 1 (as was done in Figure 3b); we can convert this into an apparent surface pressure  $\Pi_{\text{apparent}} = \sigma_0 - \sigma_{\text{apparent}}$ , where  $\sigma_0$  is the interfacial tension of the bare interface. In our case, we use the value of  $\sigma_0$  obtained from the pendant drop experiment. Combining these surface pressures with the areas of Figure 5a yields the isotherms of Figure 5b. Once again, we stress that the apparent surface pressures do not have thermodynamic significance in the jammed state; they only reflect the values calculated from the Vonnegut equation. At the highest

surface area values, the apparent surface pressures are slightly negative; this is an artifact caused by fact that the  $\sigma_0$  from the pendant drop method (17.6 mN/m) was slightly lower than the highest apparent interfacial tension measured (19.0 mN/m). With decreasing surface area, the surface pressure increases until it is equal to the interfacial tension itself. These features are qualitatively similar to the surface pressure isotherms documented for oil/water systems.<sup>9</sup> Quantitatively, however, our data show two significant differences. The first is that our isotherms stop at an area that corresponds to a jammed monolayer; unlike Langmuir trough experiments,<sup>9–12</sup> the monolayer does not further compress into a buckled state. As mentioned at the end of the previous section, when monolayer compression is driven by interfacial tension, buckling is not expected. The second significant difference is that the change from a low surface pressure to a high pressure is relatively abrupt. For the F71 drop, the apparent surface pressure rises from only 10% of its maximum value to its maximum value with a change in interfacial area of less than 20%. For the F62 drop, the transition appears even sharper; in effect, in Figure 5a, the surface area of F62 is virtually constant after jamming. It is not clear why the transition appears more abrupt for the F62 drop. Yet, it is clear that these transitions are sharper than observed previously.<sup>9,10</sup> This suggests that, in the present system, the particles do not have a strong, long-range repulsion for each other, and have a relatively “hard” interaction. Accordingly, a significant apparent surface pressure exists only when the particles are nearly in contact.

Ultimately, the phenomenon of 2D particle jamming is linked with interfacial particle concentration, rather than the interfacial area. For example, drops with a higher number of particles at the interface are expected to jam at a higher interfacial area (i.e., higher rpm) which is indeed apparent in Figures 3–5. Accordingly, Figure 6a plots the data of Figure 5a in the form of specific interfacial area (i.e., area per gram of particles), on the assumption that all the particles are at the interface. This assumption is based on two observations: (1) as mentioned in section 2.2, no particles are evident on the inner walls of the SDT tube indicating that particles do not cross the interface; (2) upon conducting the shake-and-spin procedure described in section 2.2, there was no further change in drop dimensions at a fixed rpm.

The specific interfacial area in the jammed state may be crudely estimated by assuming that the particles lie parallel to the interface in a close-packed fashion (Figure 6b). In a previous article,<sup>20</sup> based on a SEM images such as Figure 6c, we had assumed that these FeOOH particles were cuboids of dimensions  $L \times w \times w = 0.6 \mu\text{m} \times 0.12 \mu\text{m} \times 0.12 \mu\text{m}$ . These dimensions yield a close-packed specific interfacial area of 2.07 m<sup>2</sup>/g, a value illustrated by the horizontal line in Figure 6a. Figure 6a shows that the experimentally observed specific interfacial area (the plateau at low rpm) for all three drops is close to this horizontal line, suggesting that, in the jammed state, the particles are nearly tightly packed. Yet there are significant differences between the three samples: the specific interfacial area in the jammed state decreases with increasing loading. Quantitatively, the highest loading drop F71 had a 20% lower specific interfacial area (i.e., is 20% more tightly packed) than the lowest loading drop F51. It is not clear what microstructural differences may cause a more compact monolayer; considering the nonspherical shape of the particles, out-of-plane particle orientation

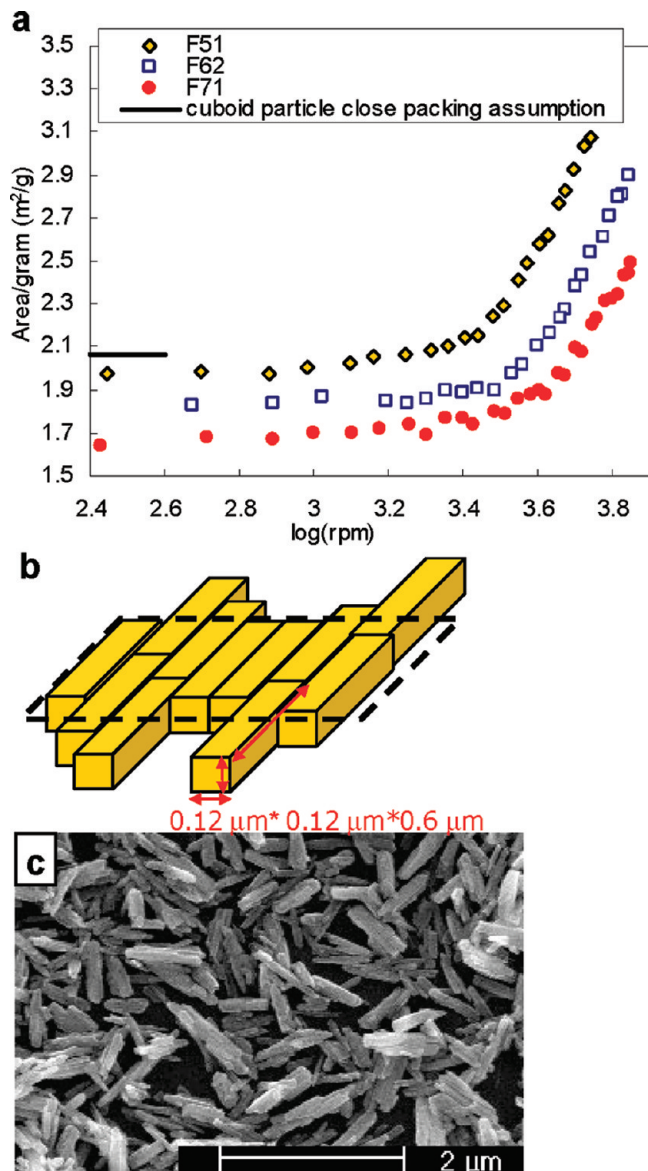


**Figure 6.** (a) Variation of specific interfacial area of particles versus  $\log(\text{rpm})$ . Solid horizontal line corresponds to 2D close packing of cuboid particles lying along the flat on interface as shown in (b). (c) SEM picture of  $\text{FeOOH}$  particles.

(“flipped” particles<sup>12</sup>) may be responsible for more compact monolayers. Certainly, it is also possible that the observed differences in specific interfacial area in the jammed state are in fact a failure of the above assumption that all particles are adsorbed at the interface.

**3.3. Effect of Rotational Rate History: Shape Hysteresis and Sudden Stepdown.** Previously, it has been noted that expansion of a monolayer can display significantly different behavior than compaction. In general, the capillary pressure during an expansion was observed to be lower than that during a preceding compression.<sup>12,14,23–25</sup> In order to examine the behavior of the present monolayers, at the end of the ratedown experiment, the F71 drop was subjected to rotation

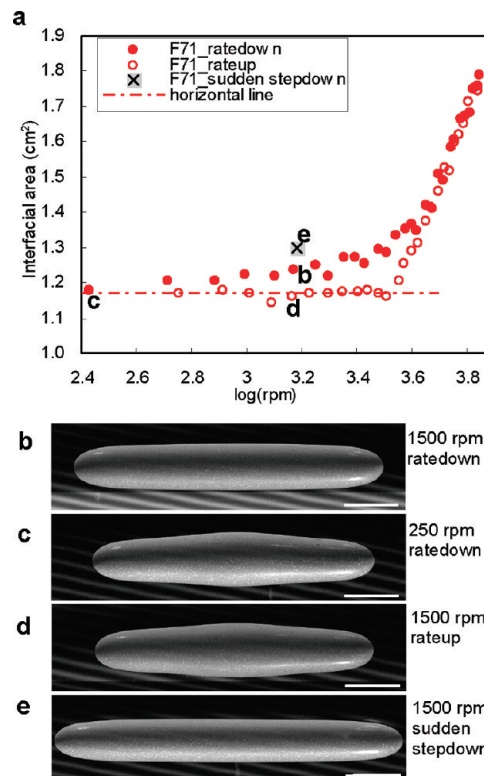


**Figure 7.** (a) Comparison of ratedown experiment, rateup experiment, and sudden stepdown experiment for F71. The images corresponding to points labeled (b), (c), (d), and (e) are below the graph. Scale bars are 3 mm.

at successively higher rates to induce re-expansion of the interface. Figure 7a compares the area of the drop during the rateup sequence with the ratedown sequence, whereas Figure 7b–d shows drop shapes at selected rpm’s in the trajectory. Significant shape hysteresis is evident in these observations. In particular, it is clear that there is essentially no change in shape when increasing the rotational speed from  $\sim 250$  rpm (Figure 7c) to 1500 rpm (Figure 7d). This is also reflected in the interfacial area, which remains virtually constant up to 3200 rpm; only above 3200 rpm does the drop shape become responsive to rotational speed, upon which the area versus rpm data of the rateup experiment rapidly approaches those of the ratedown experiment. The hysteresis, that is, the difference in drop shapes and in the drop area between Figure 7b and d, is due to the history of the sample, a situation commonly encountered in other jammed systems such as molecular glasses. The chief conclusion from this observation is that the jammed state requires a finite stress (in this case induced by centrifugal forces) to unjam and remobilize it. As in previous research, such hysteresis is likely attributable to interparticle attractions, either capillary in nature (considering the elongated shape of particles) or van der Waals. Some previous researchers<sup>12,14,24</sup> have reported that, upon expansion, the monolayer cracked, and in the expanded monolayer particle patches coexisted with particle-free bare interfaces. We have not noted cracking of the monolayers, at least at the  $\sim 50$   $\mu\text{m}$  scale resolution of our imaging.

Furthermore, we have also noted that the shape and the area of the jammed drop depends on the rate at which the interfacial area is reduced. This can be observed in a sudden stepdown experiment in which the F71 sample initially

(23) Schwartz, H.; Harel, Y.; Efrima, S. *Langmuir* **2001**, *17*(13), 3884–3892.

(24) Safouane, M.; Langevin, D.; Binks, B. P. *Langmuir* **2007**, *23*(23), 11546–11553.

(25) Horozov, T. S.; Binks, B. P.; Aveyard, R.; Clint, J. H. *Colloids Surf., A* **2006**, *282*, 377–386.

maintained at 6500 rpm was abruptly brought to 1500 rpm in about 5 s. A sequence of pictures captured during the decrease in rotational rate is available as Supporting Information. Initially, the drop starts to retract from its ends as may be expected for a particle-free drop, but the retraction is interrupted by interfacial jamming. The jammed drop resulting from this sudden stepdown (Figure 7e) is significantly more elongated than the jammed drop realized from the gradual ratedown protocol (Figure 7b) at the same rpm. More quantitatively, the interfacial area from the sudden stepdown is about 5% higher than that from a gradual ratedown experiment. The chief conclusion is that the specific interfacial area for jamming depends on the rate at which jamming is induced. Past experiments on 2D particle monolayers have sometimes noted a rate dependence of the surface pressure versus surface area isotherms,<sup>23</sup> although some experiments have noted no rate dependence.<sup>14</sup> However, we believe this is the first report in which the specific interfacial area in the final jammed state itself depends on the rate at which jamming is induced. This idea is well-established in the 3D jamming (i.e., glass formation) literature in which the specific volume of a glass depends on cooling rate.

**3.4. Nonpolar/Nonpolar System.** There is significant interest in realizing bijels in polymeric systems, in which both phases are generally relatively nonpolar.<sup>6,7</sup> Accordingly, we have also conducted limited experiments on the same particles adsorbed at the interface between silicone oil and mineral oil, a situation representative of adsorption between nonpolar phases. As mentioned in section 2.2, the interfacial tension between the equilibrated phases is on the order of 1 mN/m, which is comparable to that for many polymer pairs. In preliminary experiments, we verified partial wettability of the particles between the silicone oil and mineral oil: the particles and the two oils were blended together in a petri dish, and interfacial adsorption was clearly evident in optical images of the resulting emulsions.

Samples for SDT experiments were prepared identically to the glycol/oil case: particles were predispersed in the mineral oil, and a drop of this dispersion suspended in silicone oil was spun in the SDT to induce interfacial adsorption. A difference was immediately evident; the particles showed significant aggregation at the interface and gentle shaking of the sample tube was not able to break these aggregates. Figure 8a shows an example of the results. A patch of high particle concentration is found to coexist with a particle-free “bare” region on the interface. The fact that the particles do not exert spreading pressure at the interface suggests that interparticle repulsions are weak. This is not surprising: since both phases have low polarity, the particles are not expected to have significant charge, and hence, electrostatic repulsion is likely to be absent. Accordingly, the interparticle attractions (likely capillary in nature given the nonspherical particle shape<sup>26</sup>) dominate, causing interfacial aggregation. It is also noteworthy that the particle loading in Figure 8a was adequate to cover the surface area of this drop (assuming the same specific interfacial area of 2.07 m<sup>2</sup>/g estimated in the previous section). This clearly indicates that some particles either are adsorbed in an out-of-plane “flipped” configuration, or are not adsorbed at the interface but remain in the bulk. If the latter is true, then the particles in the bulk are likely associated with those at the

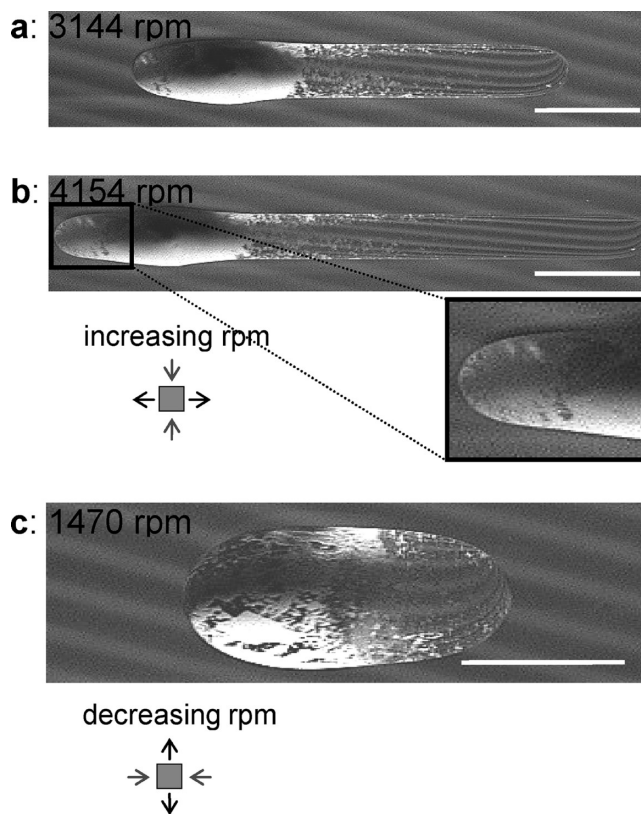


**Figure 8.** (a) Particles adsorbed at the interface between mineral oil and silicone oil. (b) Same drop upon increasing rotational speed. (c) Same drop upon decreasing rotational speed. Scale bars are 3 mm.

interface since gentle shaking of the tube did not increase the particle adsorption.

Upon changing the rotational rate, the attraction-dominated monolayer behaves significantly differently from the previous glycol/oil case. Increasing the rpm (Figure 8b) causes the bare portion of the interface to elongate unhindered, but the particle-covered patch extends only slightly with cracks developing perpendicular to the axial (stretching) direction. Correspondingly, decreasing the rpm causes drop retraction, with cracks appearing azimuthally, again perpendicular to the stretching direction. It is noteworthy that as the rpm is increased or decreased, the particle-free portion of the drop stretches and contracts as expected quite independently of the particle-covered patch.

#### 4. Conclusions

We have examined interfacial particle jamming using a spinning drop tensiometer (SDT) for the first time. By reducing the rotational speed of the spinning drop, its interfacial area can be reduced in a controlled fashion. Since this decrease in interfacial area occurs due to capillary pressure, it is representative of the jamming process in bijels.

For FeOOH particle monolayers adsorbed at the oil/glycol interface, our experiments show that drops maintain a non-spherical shape when the particle coverage becomes sufficiently high; furthermore, elongated drops are also stable against capillary instabilities. In contrast to past experiments using Langmuir troughs or a shrinking drop, interfacial buckling was not observed, and we believe that lack of buckling is a general feature of interfacial tension-driven jamming. Calculations indicate that the specific interfacial area for jamming is close to that expected for a tightly packed monolayer of particles.

(26) Loudet, J. C.; Alsayed, A. M.; Zhang, J.; Yodh, A. G. *Phys. Rev. Lett.* **2005**, *94*(1), 018301.

However, the specific interfacial area varies by as much as 20% with changes in particle loading. Furthermore, there was significant hysteresis between compressing versus expanding the jammed monolayer, which suggests that a certain minimum force is required for unjamming. Finally, rapid interfacial contraction led to a less tightly packed monolayer in the jammed state, a behavior similar to glass formation.

Finally, limited experiments on the same particles adsorbed at the interface between two nonpolar liquids (mineral oil and silicone oil) show altogether different behavior. The particles do not spread at this interface but instead form a high concentration jammed patch that coexists with a particle-free region of the interface. This suggests that interparticle

repulsion is weak in this nonpolar system and hence monolayer behavior is dominated by interparticle attraction.

**Acknowledgment.** This research was supported by a CAREER grant CBET-0448845. The authors thank Elementis Pigments Inc. for FeOOH particles. The authors thank Dr. Cheng-Chun Chang for the assistance in writing the Matlab codes for surface area and volume calculation.

**Supporting Information Available:** Sequence of pictures captured during the sudden decrease in rotational rate. This material is available free of charge via the Internet at <http://pubs.acs.org>.